4

3-D Ultrahigh Resolution Optical Coherence Tomography with Adaptive Optics for Ophthalmic Imaging

Guohua Shi*, Jing Lu, Xiqi Li and Yudong Zhang
Institute of Optics and Electronics,
Chinese Academy of Sciences,
Shuangliu, Chengdu,
P R China

1. Introduction

By use of broad bandwidth light source, the potential of OCT is demonstrated to perform noninvasive optical biopsy of the human retina (D. Huang, et al, 1991). OCT is based on low coherence interferometry (R. C. Youngquist, et al, 1987), in which the pattern of interference between the reference and object beams is used to determine the amount of light reflected back from a certain point within the volume of the sample under study. The broad bandwidth source is used for illumination, so the two beams only produce an interference pattern when their optical paths difference is less than the coherence length of the source. This means that the bandwidth of the source determines the axial resolution of the OCT system. Therefore, by using ultra-broad bandwidth light source (such as Ti: Al2O3 laser, laser generated from a photo crystal fiber, ultra-broadband SLD), the cross section image as biopsy is achieved successfully(A. Unterhuber, et al, 2003, Yimin Wang, et al, 2003, D.S. Adler, et al, 2004).

The transverse resolution in ophthalmic OCT is determined by beam-focusing conditions on the retina (Bratt E. Bouma, et al, 2002). The smaller achievable spot size means the higher transverse resolution. For an ideal eye, a large diameter beam would produce a small theoretical spot size. However, in practice, for large pupil diameters, mono-chromatic aberrations of the human eye blur the retinal images. Although the axial resolution of ophthalmic OCT has been improved dramatically, the transverse resolution is still limited to 15-20 μm in retinal ultra high resolution OCT (UHR OCT) tomograms because of the small pupil diameter used.

Adaptive optics (AO) can correct the aberration in real time. By using adaptive optics, the optical resolution of retina camera is significantly increased by correcting the ocular aberrations across a large pupil. Combined OCT with AO, 3-D ultrahigh resolution is achieved. The increase of transverse resolution permits the observation of human retinal structures at the cellular level in vivo.

* Corresponding Author

2. Resolution of OCT

Unlike conventional microscopy, the axial and transverse optical resolutions of OCT are independent, because of its unique mechanism. Either Time Domain OCT or Fourier Domain OCT, the axial resolution for OCT imaging is determined by the coherence length of the illumination source (R. Leitgeb, et al, 2003). Therefore, the shorter the coherence length, the higher the axial resolution is. Thus, the axial resolution is inversely proportional to the bandwidth of light source. Assumes a Gaussian spectral illumination source, the axial resolution Δz is

$$\Delta z = \frac{2\ln 2}{\pi}\left(\frac{\lambda_0^2}{\Delta\lambda}\right). \tag{1}$$

Where λ_0 is the center wavelength of the illumination source and Δλ is the 3dB bandwidth of tits spectrum. Equation (1) reveals that to increase axial resolution the broad band spectral sources is required. By use of ultra-broad bandwidth light sources, the ultrahigh axial resolution optical coherence tomography can be achieved.

While the axial resolution in OCT is governed by the source coherence length, OCT's transverse resolution is the same as optical microscopy, and is determined by the focusing properties of the illumination beam which is limited by diffraction and aberrations of optical system (Born. M and Wolf. E, 1980). Ideally, the transverse resolution is

$$\Delta x \approx 1.22\lambda_0\left(\frac{f}{d}\right). \tag{2}$$

Where f is the focal length of objective and d is its effective aperture. Theory, by using high NA objective to focus a small spot size, the high transverse resolution can be achieved. In practice, when the case of a fixed numerical aperture, the optical system aberration determine the focus size.

The transverse resolution in ophthalmic UHR OCT is constrained by the pupil size of eye, which determines smallest achievable spot size on the retina. However, in practice, human eyes is not a perfect optical system for large pupil diameter, it has wave front aberrations which deteriorate the transverse resolution of OCT (Junzhong Liang, et al, 1993). Although the axial resolution of ophthalmic OCT has been improved dramatically, the transverse resolution is still limited to 15-20 μm in retinal UHR OCT tomograms because of the small pupil diameter used (H.C. Howland, et al, 1977).

3. Wave front aberrations of human eye

3.1 Zernike mode aberrations

We can use the wave front aberration to describe the transverse imaging properties of ophthalmic imaging optical system perfectly. It is defined as the optical path difference (OPD) between the perfect spherical wave front and the actual wave front for every point over the eye's pupil. The ideal eye focuses a perfect spot (Airy disk) on retina. Actually, the existence of eye's wave front aberration blur the focused spot on retina significantly (J. Liang, et al, 1997).

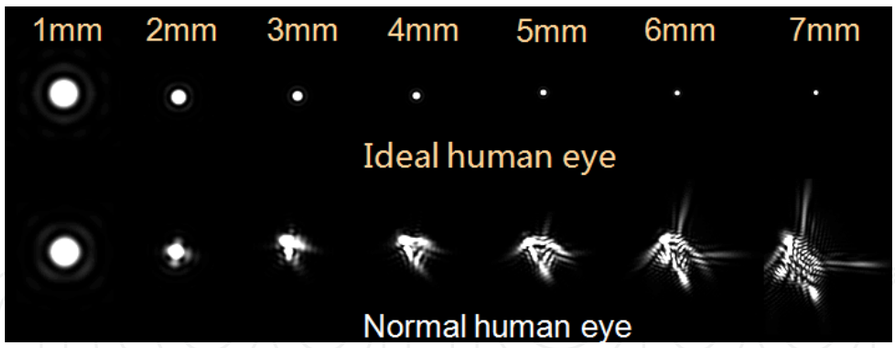

Fig. 1. The ideal and reality PSF change with pupil size.

Fig 1 shows the ideal and reality PSF that change with pupil size. In theory, with the increase of pupil size, the ideal PSF will rapidly become smaller because of the diffraction effects. It's mean the improvement of transverse resolution. In fact, for a normal human eye (without refractive disease) the reality PSF will became smaller at first, and will achieve the minimum when the pupil size is 3mm. Because the smaller pupil size means the smaller wave front aberration. Then, with the increase of pupil size, the wave front aberrations increased dramatically, so the reality PSF become rapidly expanding.

Fortunately, most of normal human eyes just have the 3mm pupil size. But for ophthalmic imaging, transverse resolution of 3mm pupil size is not enough. Therefore, the key issue is how to correct the wave front aberration which is introduced by the large pupil. The wave front aberration may be mathematically represented and broken down into its constituent aberrations (such as defocus, astigmatism, coma, spherical aberration, etc.) using a Zernike decomposition.

$$\varphi(\vec{r}) = \sum_{k=1}^{N} a_k Z_k(\vec{r}) \tag{3}$$

Where $\varphi(\vec{r})$ is the wave front phase. $Z_k(\vec{r})$ and a_k is the Zernike mode and its corresponding coefficient. Zernike polynomials are set of orthogonal polynomials on a circular domain. It is defined as

$$Z_k = \begin{cases} \left.\begin{array}{l} \sqrt{2(n+1)}R_n^m(\rho)\cos(m\theta).....k = odd \\ \sqrt{2(n+1)}R_n^m(\rho)\sin(m\theta).....k = even \end{array}\right\}.....m \neq 0 \\ \sqrt{n+1}R_n^m(\rho).....m = 0 \end{cases} \tag{4}$$

Where $R_n^m(\rho)$ is

$$R_n^m(\rho) = \sum_{s=0}^{(n-m)/2} \frac{(-1)^s (n-s)!}{s!\left(\frac{n+m}{2}-s\right)!\left(\frac{n-m}{2}-s\right)!}\rho^{n-2s} \tag{5}$$

Where m and n is angular frequency and the radial frequency separately. They are constant integers and satisfy

$$m \le n, n - |m| = even; \tag{6}$$

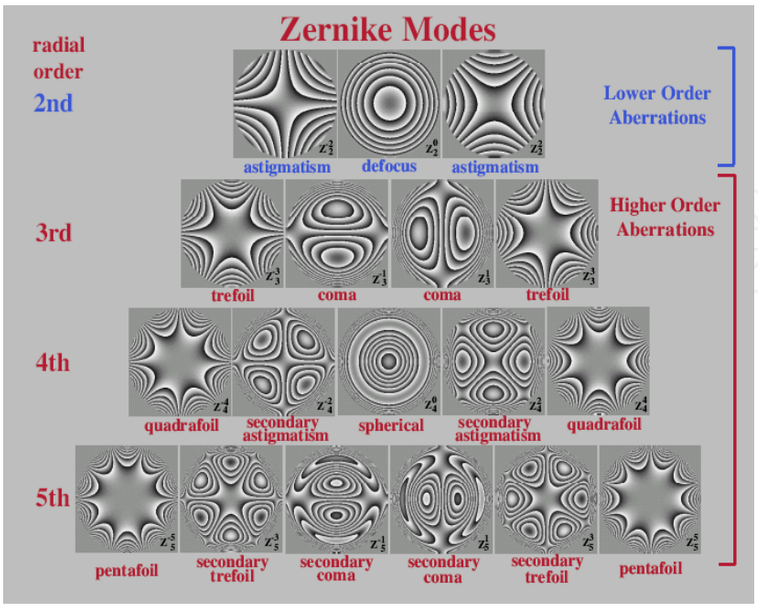

Fig. 2. The Zernike modes wave front aberrations

Fig. 2 and 3 shows the Zernike modes wave front aberrations and its corresponding point spread function (PSF). Glasses and contact lenses have been used to correct the lower order aberrations (defocus and astigmatism) of eye. However, it has been well known that the human eye also suffers from the higher order aberrations, in addition to typical defocus and astigmatic errors. Moreover the higher order aberrations different from each subject, and change over time. So it is impossible to solve higher order aberrations by optical design.

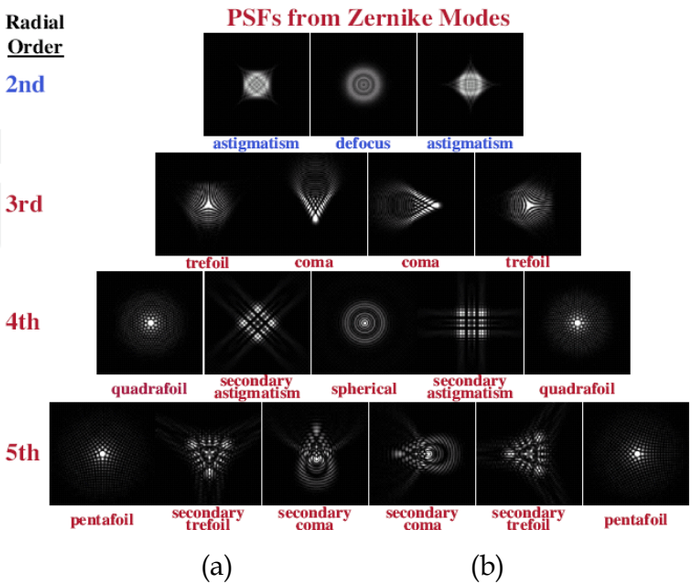

Fig. 3. The PSF of each Zernike modes wave front aberration.

3.2 Hartmann-Shack wave front sensor

In order to correct the wave front aberrations of the eye, we must measure the aberrations at first. In reality, every refracting ocular surface generates aberrations, and they contribute differently to the overall quality of the retinal image. The monochromatic aberration of the complete eye, considered as one single imaging system, can be measured using a large variety of wave front sensing techniques. However, from 1994, with the development of human eye Hartmann-Shack wave front sensor, the researchers of the human eye wave front aberration have a more in-depth understanding, recognizing that the human eye aberrations in addition to defocus, astigmatism, but also there are other more complex higher-order aberrations (J. Liang, et al, 1994, Ning Ling, et al, 2001, Heidi Hofer, et al, 2001).

Figure 4 shows the measuring principle of Hartmann-Shack wave front sensor (Ning Ling, et al 2001). The Hartmann-Shack wave front sensor is consist of a micro-lens array and a CCD camera. The incident wave front is divided into several sub-apertures by micro lens array, then image by CCD camera.

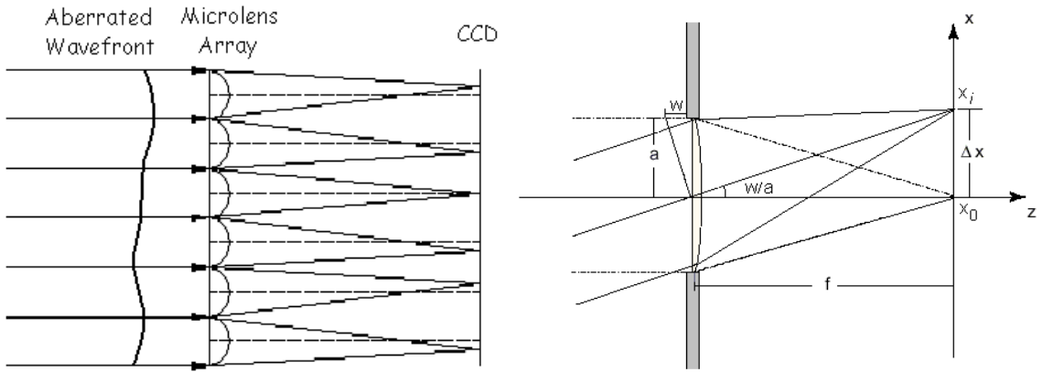

(a) (b)

Fig. 4. (a) The schematic diagram of Hartmann-Shack wave front sensor; (b) Focal spot displacement caused by the incident wave front tilt

If the incident wave front is ideal plane wave front, set the centroids of sub-apertures focal spots as reference position (x0, y0). When the incident wave front have aberrations, then the centroids of sub-apertures focal spots (xi, yi) will deviate from reference position. The offsets of X and Y direction are proportional to the X and Y directions average slope of the wave front. Wave front slope (in wavelength/sub-aperture unit) can be expressed as

$$g_{xi} = \frac{x_i - x_o}{\lambda f} = \frac{\iint \frac{\partial \varphi(x,y)}{\partial x} ds}{\iint ds}, \quad g_{yi} = \frac{y_i - y_o}{\lambda f} = \frac{\iint \frac{\partial \varphi(x,y)}{\partial y} ds}{\iint ds} \tag{7}$$

Where φ(x, y) is the phase of incident wave front, f is the focal length of micro lens array, and λ is the wavelength of incident light.

After obtain the sub-aperture wave front slope, the wave front reconstruction algorithm can calculate the phase distribution function φ(x, y). There are many kinds of wave-front reconstruction algorithm that can be used in different applications. In order to measure

higher-order aberrations for the human eye, Zernike wave front reconstruction mode method is more appropriate.

Through the derivative of Zernike polynomials and within each sub-aperture averaging, the average slope of the sub-aperture can be established the relationship with the Zernike mode coefficients.

$$\begin{cases} g_{x_m} = \sum_{n=1}^{N} a_n \dfrac{\iint_{\sigma_m'} \dfrac{\partial Z_n(x,y)}{\partial x} dxdy}{\iint_{\sigma_m'} dxdy} \Bigg|_m \\ g_{y_m} = \sum_{n=1}^{N} a_n \dfrac{\iint_{\sigma_m'} \dfrac{\partial Z_n(x,y)}{\partial y} dxdy}{\iint_{\sigma_m'} dxdy} \Bigg|_m \end{cases}, \tag{8}$$

Where σ_m is the corresponding integral area of the detected aperture M on the unit circle. Write the all the sub-aperture's slope and the Zernike mode coefficient in vector form.

$$\begin{aligned} \vec{g} &= \left(g_{x_1}, g_{y_1}, g_{x_2}, g_{y_2}, \ldots\ldots, g_{x_M}, g_{y_M}\right)^T \\ \vec{a} &= \left(a_1, a_1, \ldots\ldots a_N\right)^T \end{aligned} \tag{9}$$

Where $\vec{g}$ is slope vector and $\vec{a}$ is Zernike mode coefficient vector. Then the Eq. (8) can be written

$$\vec{g} = D\vec{a} \tag{10}$$

Where D represents the relationship matrix of slope vector $\vec{g}$ and Zernike mode coefficient vector $\vec{a}$. So the generalized inverse of D is the wave front reconstruction matrix of Zernike wave-front reconstruction mode method. Thus, the Zernike mode coefficient vector $\vec{a}$ can be obtain by

$$\vec{a} = [(D^T D)^{-1} D^T] \cdot \vec{g} = D^+ \cdot \vec{g}$$

Using Zernike mode coefficient vector $\vec{a}$, we can calculate the phase distribution function φ(x, y), get the Zernike wave front aberrations, calculate the PSF of whole optical system.

Fig. 5 is the results of a volunteer measured by H-S sensor in our lab (Ning Ling, et al 2001). H-S sensor can not only achieve the wave front measurement of eye, but aslo can get the system PSF, MTF, encircled energy. And it measures in real time, thus can measure the wave front aberrations changes with time. International Organization for Standardization have recommended Zernike polynomial to describe wave front aberrations of human eye. So H-S sensor has become the most important techniques of optometry research.

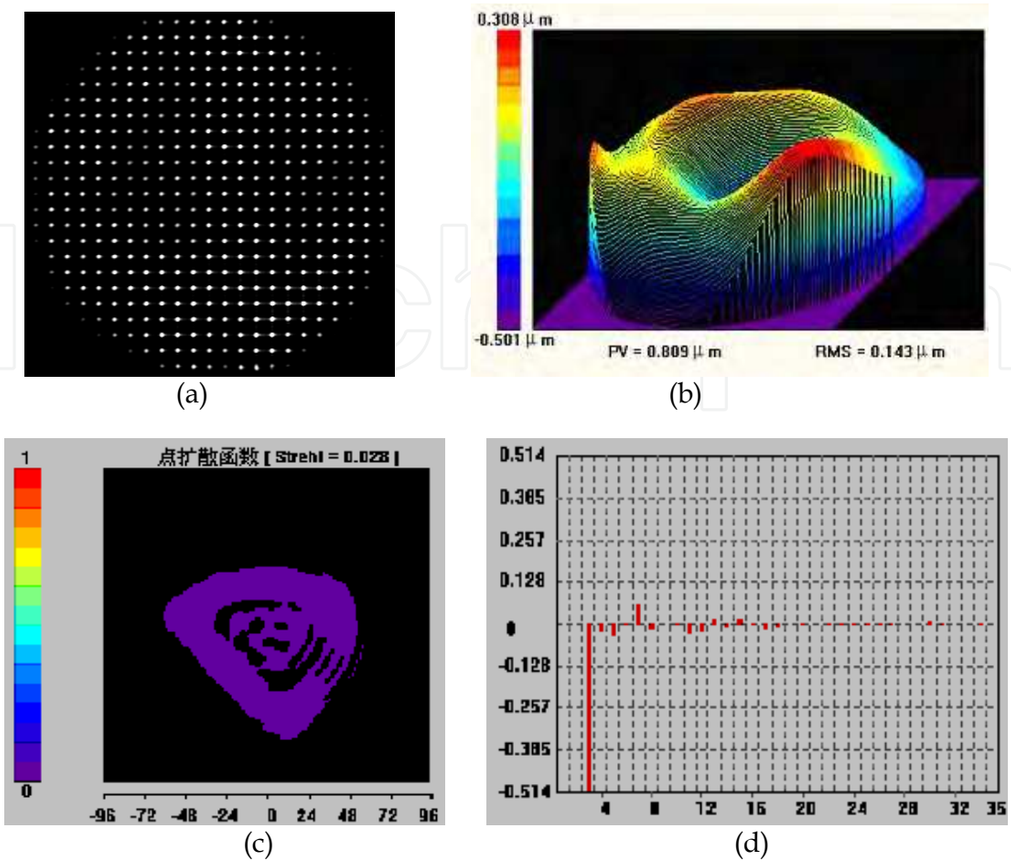

Fig. 5. (a) is the spot array of a volunteer obtained by H-S sensor; (b) is the wave front reconstructed by Zernike wave-front reconstruction mode method; (c) is the PSF of volunteer eye; (d) is the first 35 order Zernike coefficient

4. Principle of adaptive optics

4.1 Wave front corrector

When the wave front aberrations of the eye are measured precisely and in real time, it is possible to correct them by using a wave front correcting device that compensates the eye's aberrations. This is a direct application of Adaptive Optics (AO) on the eye imaging. In the ideal case, the AO system produces retinal images with perfect transverse resolution.

Adaptive optics was first used in large astronomical telescopes (Fried D L, 1997), which includes wave front sensor, wave front corrector and control system. Fig. 6 is the typical adaptive optics system. The basic principle of adaptive optics is phase conjugation (R.K.Tyson, 1991). The electric field of an incident light can be expressed as

$$E_1 = |E| e^{i\varphi} \tag{12}$$

Where the φ is the phase of incident light and it is affected by external disturbance, such as temperature variation, atmospheric turbulence, eye aberrations and so on. The function of

adaptive optics system is to produce phase that is the conjugate of the incident light. Thus, the phase error (wave front aberration) is compensated, and the incident light became an ideal plane wave. This lead to a diffraction limit resolution image.

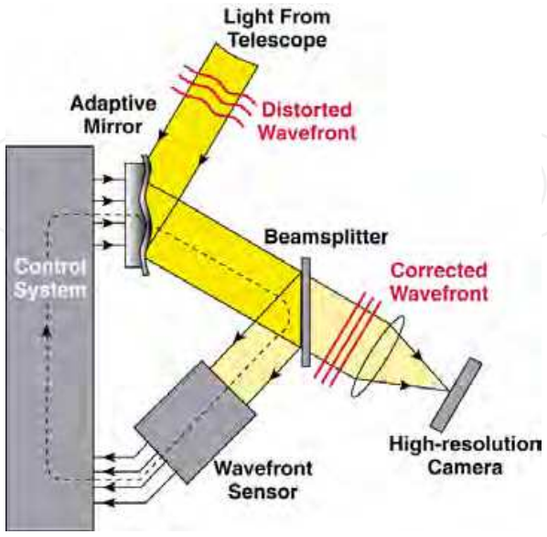

Fig. 6. Schematic diagram of a typical adaptive optics system.

Wave front corrector is the core component in adaptive optics system. It determines the performance, size and cost of the adaptive optics. The wave front corrector changes its surface by driving the actuators push or pull the thin mirror. This produces an opposite wave front phase which is measured by wave front sensor to correct the aberrations of optical system. Different types of wave front corrector have been used to correct eye's aberrations, such as liquid crystal spatial light modulators (E.J. Fernandez, et al, 2005), micro-mechanical deformable mirror (Y. Zhang, et al, 2006), bimorph deformable mirror (Robert J. Zawadzki, et al 2005) and deformable mirrors (Yudong Zhang, et al 2001). Their pictures are shown in Fig. 7.

Type	No. of the actuators	Stroke	Size	Cost
liquid crystal spatial light modulator	800×600	One wavelength	21 x 26 mm	lower
micro-mechanical deformable mirror	12×12	3μm	4mm×4mm	lower
bimorph deformable mirror	35	32μm	10mm	expensive
deformable mirror	37	4μm	Ø40mm	Most expensive

Table 1. Comparison of four wave front corrector.

Table 1 is the comparison of four types of wave front corrector. Liquid crystal spatial light modulator has the minimum stroke, which is just one wavelength, and it has the lowest optical power efficiency. Micro-mechanical deformable mirror is low cost and small size, but its stroke (3-6μm) is not enough for correcting large aberrations. Though deformable mirror is the wild used wave front corrector, but its bulky size and expensive cost restricts its

application for retinal imaging. Synthetically, the bimorph deformable mirror is the cost-effective wave front corrector.

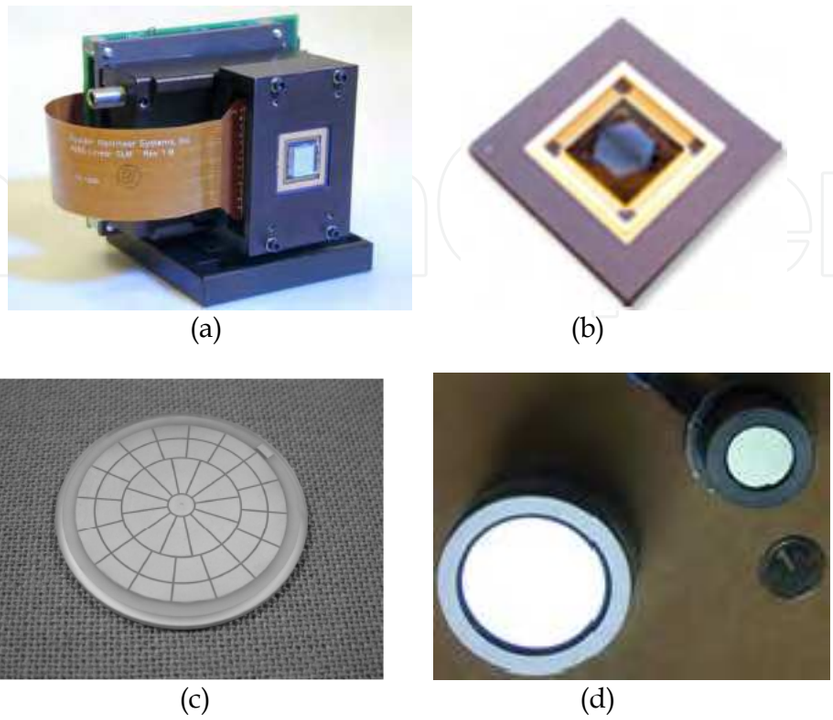

(a) (b)

(c) (d)

Fig. 7. Pictures of four wave front corrector. (a) liquid crystal spatial light modulator; (b) micro-mechanical deformable mirror; (c) bimorph deformable mirror; (d) deformable mirror.

4.2 Direct slope method for adaptive optics

Except liquid crystal spatial light modulator, the other wave front correctors correct aberrations by applying voltage to actuators to change surface shape of the thin mirror. Thereby, the control algorithm is important because it is the vital link between the wave front sensor and the wave front corrector in an adaptive optics system. According to Eq. (11) can reconstruct incident wave front. But calculating each actuator's drive voltage from the reconstructed wave front require complex decoupling algorithm, which is a complex process. Direct slope method is the most widely applied control algorithm (Wenhan Jiang, Huagui Li, 1990). It uses the wave front slope as control variables instead of wave front phase. So it is particularly suitable for the AO system that include H-S wave front sensor.

Assuming an ideal optical system, the sub-aperture of H-S sensor detects the slop generated by wave front corrector. So the slop of x and y direction in the i th sub- aperture is

$$\begin{aligned} G_{xi} &= \sum_{j=1}^{n} V_j R_{xij} \\ G_{yi} &= \sum_{j=1}^{n} V_j R_{yij} \end{aligned} \qquad \text{i=1,2,3,4……n} \tag{13}$$

Where R_{xij} and R_{yij} are the slop of x and y direction in the i-th sub-aperture when the j-th actuator applied unit drive voltage alone. V_j is the drive voltage of the j-th actuator. n is the number of actuator. Therefore, Eq. (13) can be expressed as

$$G = DV \tag{14}$$

D is called influence function slope matrix and its elements are R_{xij} and R_{yij}. It is determined by adaptive optics system itself, and can be measured by adaptive optics system itself too. Wave front slop vector G is measured by wave front sensor, which is defined as Eq. (9) shows. V is the drive voltage matrix. So, using least square method, V is

$$V = D^{+}G \tag{15}$$

Where D^{+} is the generalized inverse matrix of D, and called as control matrix. When the AO system is working, the H-S sensor measures the slop of incident wave front. Then according to Eq. (15), we can get the drive voltage and control the wave front corrector to correct the wave front aberration.

5. Adaptive optics optical coherence tomography

University of Rochester take the lead in the use of adaptive optics for ophthalmic imaging (D. T. Miller et al, 1996, J. Liang, et al, 1997). They combined the AO with fundus camera. By using AO to correct the aberration caused by large pupil size (6 mm), the transverse resolution of fundus camera achieved 2μm, and imaged three cone classes in the living human eye successfully (Austin. Roorda & DavidR.Williams, 1999). But the axial resolution of AO- Camera is lower, so the AO-CSLO (Adaptive Optics Confocal Scanning Laser Ophthalmoscope) and AO-OCT (Adaptive Optics Optical Coherence Tomography) have been invented one after the other (A.Roorda, et al, 2002, D. T. Miller, et al, 2003).

Fig. 8 shows the 3-D PSF comparison of AO-Camera, AO-CSLO and AO-OCT. The width and height of the scale bar represent the axial and transverse resolution separately. So it is clear that AO-OCT have the smallest 3-D PSF. Thus, AO-OCT is the highest resolution for ophthalmic imaging in vivo so far. Since 2003, many research groups carried out the study of AO-OCT, and realized the 3-D imaging of different kinds of human retinal cell in vivo.

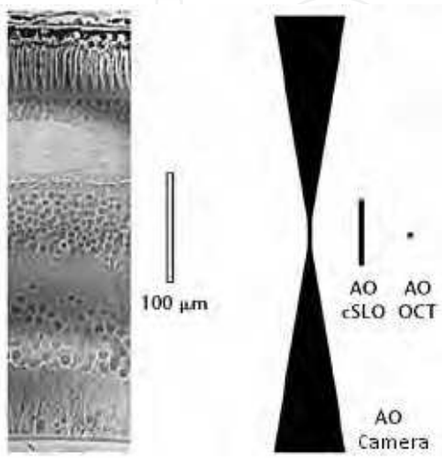

Fig. 8. The 3-D PSF comparison of ophthalmic imaging techniques.

5.1 Adaptive optics combined with time domain OCT

In 2003, D. T. Miller et al. have been first tried to combine an enface coherence gated camera with AO for enface OCT imaging with axial resolution (2μm) and high transverse resolution, and obtained the images of in vitro bovine retina (D. T. Miller, et al, 2003). In 2004, B. Hermann merged the ultrahigh-resolution time domain optical coherence tomography (UHROCT) with adaptive optics (AO), resulting in high axial resolution (3um) and improved transverse resolution (5-10 um) is demonstrated for the first time in human retinal imaging in vivo (B. Hermann, et al, 2003).

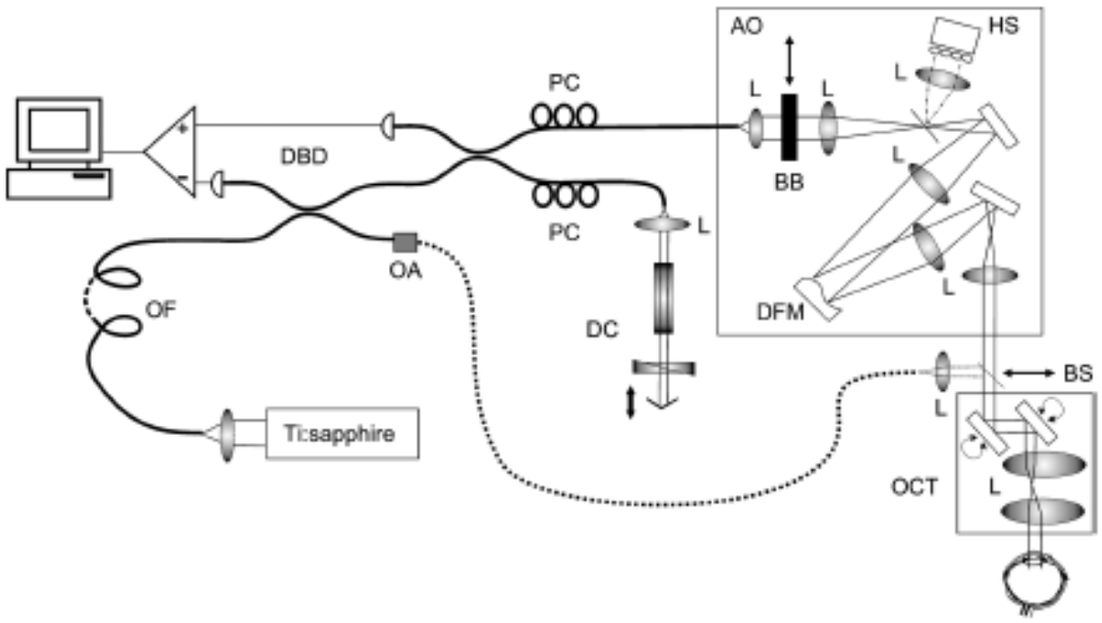

Fig. 9. The AO-OCT system which is developed by B. Hermann, et al, in 2003. DBD, dual balanced detection; PCs, polarization controllers; OA, optical attenuator; OF, 100 m of optical fiber; DC, dispersion compensation; L's, achromatic doublet lenses; BB, removable beam blocker; DFM, deformable mirror; BS, removable beam splitter.

Fig.9 is the schematic diagram of B. Hermann's AO-OCT system. A closed-loop AO system, based on a real time Hartmann–Shack wave front sensor operating at 30Hz and a 37-actuator membrane deformable mirror, is interfaced to an UHR OCT system, based on a commercial OCT instrument, employing a compact Ti: sapphire laser which's center wavelength is 800 nm with 130 nm bandwidth. The AO system was designed to conjugate the exit pupil of the eye on to the deformable mirror, in to the H-S sensor. The diameter of the measurement beam entering the eye was increased from 1mm to 3.68mm. When the correction was achieved, the system was switched to the UHR OCT imaging mode by removal of the beam blocker and the beam splitter.

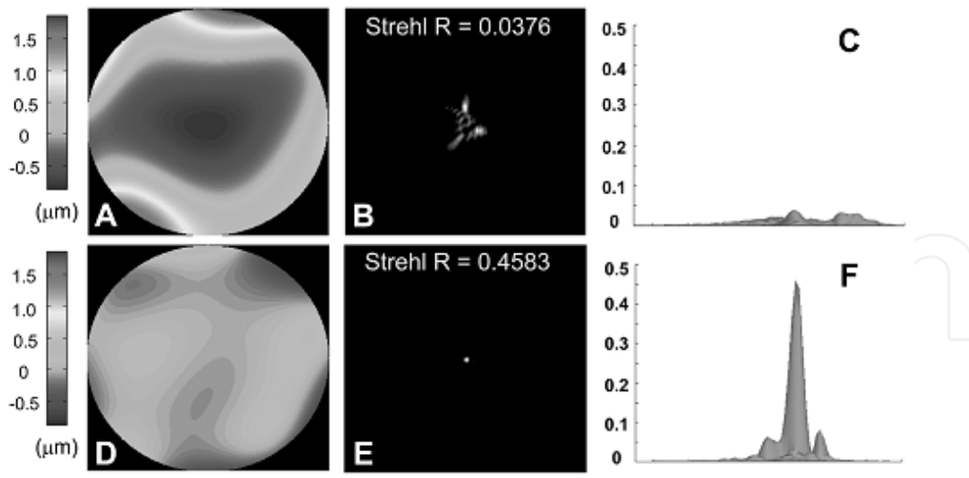

Fig. 10. Wave front for the A, uncorrected and D, corrected case and the associated PSFs for the B, C, uncorrected and E, F, corrected cases are indicated.

After corrected the eye aberration by AO, the residual of uncorrected wave front aberration is 0.1um (see Figs. 10A and 10D)., and the Strehl ratio improvements of a factor of more than 10 (Figs. 10B and 10E) were achieved, resulting in a significantly improved PSF profile (Figs. 10C and 10F). Fig. 11 illustrates the significantly effect of aberration correction in AO UHR OCT image.

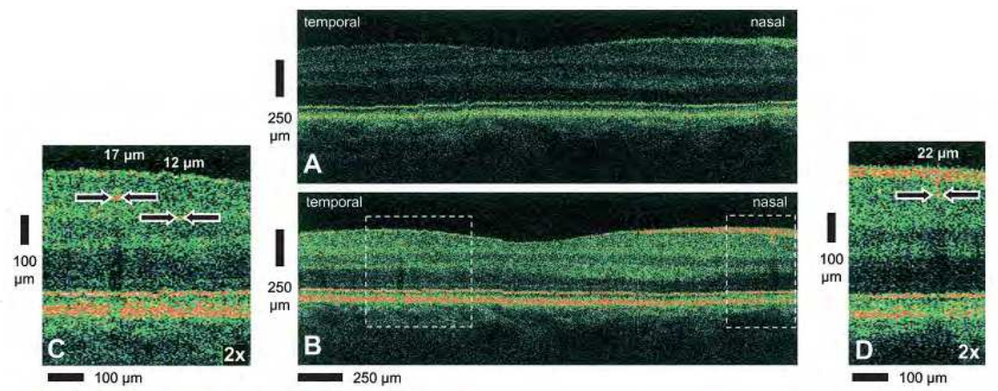

Fig. 11. In vivo AO UHR OCT tomograms of a normal human eye in the foveal region for the A, uncorrected as well as B, corrected case (600 A-scans over a line of 2.8 mm, transverse sampling rate of ~5μm). B, SNR improvement of up to 9 dB as well as 5-10μm transverse in addition to 3μm axial resolution could be achieved by wave-front corrections introduced by a 3.68 mm diameter beam. C, D, Small features within the ganglion cell layer, as well as inner plexiform layer, that might correspond to vessels with 12-22μm diameter are clearly visualized in twofold enlargements.

Guohua Shi et al have used AO to correct the aberration of a 6mm pupil size to improve the transverse resolution furthermore (Shi Guohua, et al, 2007 and 2008). But the earlier AO-OCT system combined AO with TD-OCT, so the imaging speed is slow. As the reference shows the fastest A-scan rate of TD-OCT is 8KHz (A.M. Rollins, 1998). Therefore, although

using AO to correct the aberration of a 6mm pupil size, the AO-TDOCT can't achieve the 3-D image mosaic of retinal tomography image, because of the human eyes jitter. Thus, the AO-TDOCT system can't provide the high resolution C-scan OCT image of retinal cell. In addition, the wave front sensor is very sensitive to the back-reflections from the lenses of the optical system. So the optical system must use off-center illumination geometry, and this increases the difficulty of optical adjustment.

5.2 Adaptive optics combined with spectral domain OCT

The combination of AO and TD-OCT, a resolution approaching a few microns in three dimensions is possible. With the development of Fourier Domain OCT the imaging speed and signal-to-noise ratio have a greatly improved (R. Leitgeb, et al, 2003, J.F. de Boer, et al, 2003). This provides a technical approach to overcome the retinal jitter to achieve en-face OCT image of retinal cells. In 2005, AO has been combined with free space parallel SD-OCT and fiber based SD-OCT (R. Zawadzki, et al, 2005, Y. Zhang, et al, 2005). These instruments have been reported to achieve lateral and axial resolutions up to 3μm and 2-3μm in the eye, respectively. The instruments, however, were tailored for specific experiments that did not emphasize volumetric imaging of single cells.

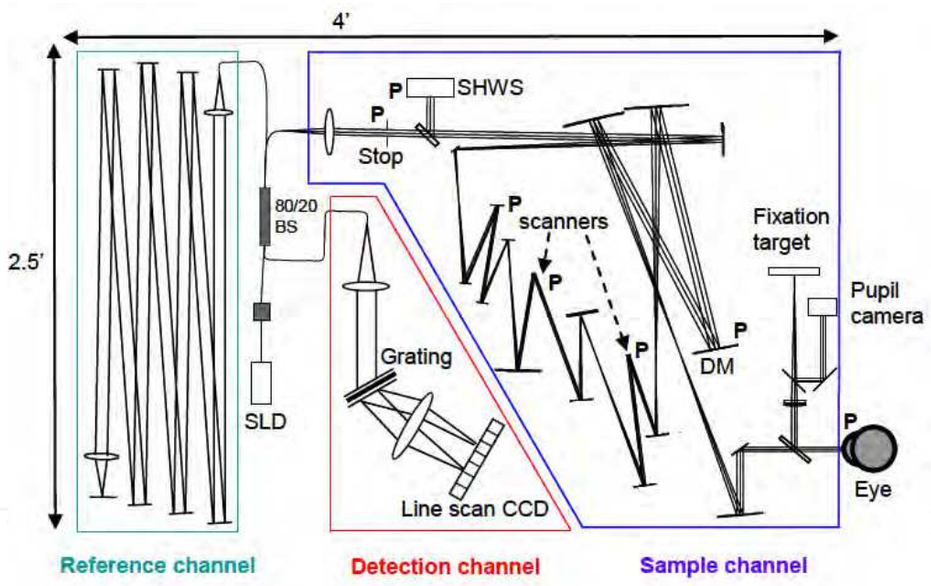

Fig. 12. Layout of the AO- SDOCT retina camera. The camera consists of three channels: (1) sample channel, (2) reference channel, and (3) detection channel. The AO system is integrated into the sample channel. BS, DM, and P refer to the fiber beam splitter, AOptix deformable mirror, and planes that are conjugate to the pupil of the eye, respectively.

In 2006, Yan Zhang established an AO-SDOCT (adaptive optics spectral domain optical coherence tomography) system for high-speed volumetric imaging of cone photoreceptors (Yan Zhang, et al, 2006). In order to overcome retinal jitter, the SDOCT components based on a fast line scan camera which's A-scan rate is 75KHz, and a shorter distance of raster scans (38 A-scans per B-scan). Thus, retinal motion artifacts were minimized by quickly acquiring small volume images of the retina with and without AO compensation. Fig. 12 is

the layout of its system. A SLD (λ_0= 842 nm, $\Delta\lambda$ = 50 nm) illuminates the retina. In the sample arm, it uses reflective optics to minimize the back-reflections of the optical system. The pupil of the eye conjugated to the wave front corrector (an AOptix deformable mirror has 37 actuators with a maximum stroke of 32μm for defocus correction), the X-Y scanner and the 20×20 lenslet array of the H-S sensor. The closed-loop rate of AO components is 12 Hz.

The result of correcting aberration shows as Fig. 13(a). AO compensation clearly reduces the magnitude of the aberrations and increases the Strehl ratio at the SLD wavelength of 842nm from 7% to 35%. As an alternative image quality metric, Fig. 13(b) shows a root mean square (RMS) trace of the measured wave aberrations for the same subject before and during AO dynamic correction. By correcting the wave front aberration of 6.6mm human eye pupil size, the transverse resolution is 3μm.

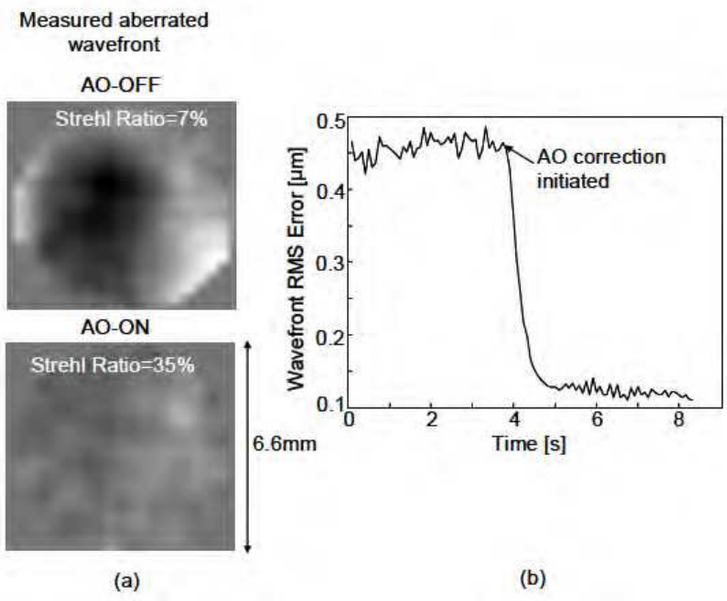

Fig. 13 (a) Residual of wave front aberrations across a 6.6 mm pupil in one subject as measured by the H-S sensor before and after AO compensation. Wave front phase is represented by a gray-scale image with black and white tones depicting minimum (-1.0μm) and maximum (1.19μm) phase, respectively. (b) An RMS trace of the residual wave aberrations is shown for one subject before and during dynamic AO correction.

Figure 14 shows C-scan image in vivo at the posterior tips of the OS with and without AO working. The volume images is a small patches of 2° retinal eccentricity retina which is 38×285×1100μm (width × length × depth) with a sampling density of 1×1×2.2μm duration of 150ms. The Fig.14 demonstrated that the AO-SDOCT was necessary for observing individual cone photoreceptor cells and led to a significant increase in the SNR (about 7-8dB) in C-scan images.

In recent years, there has been a variety of AO-SDOCT device. David Merino et al use adaptive optics to enhance simultaneous en-face optical coherence tomography and scanning laser ophthalmoscopy (David Merino, et al, 2006). RobertJ. Zawadzki et al

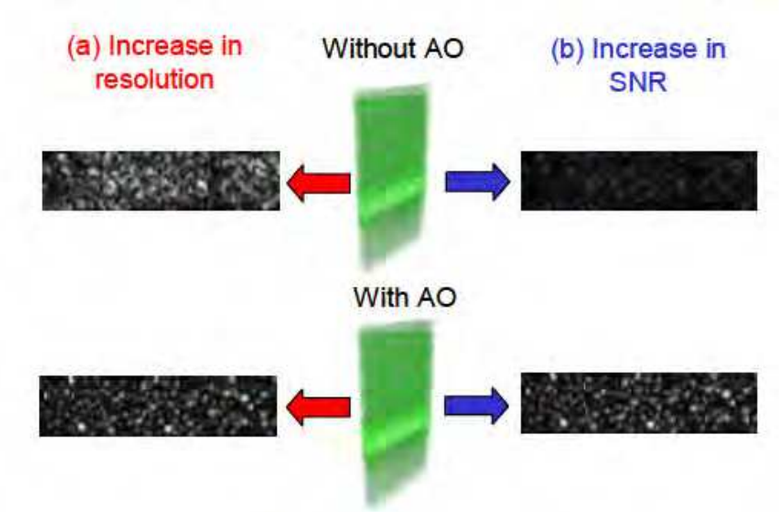

Fig. 14. (a) C-scan images at the posterior tips of the OS show an increase in transverseresolution with AO. The two images are normalized to their own gray scale so as to permit better visualization of the cone photoreceptor structure. (b) The same C-scan images in (a), but adjusted to the same gray scale.

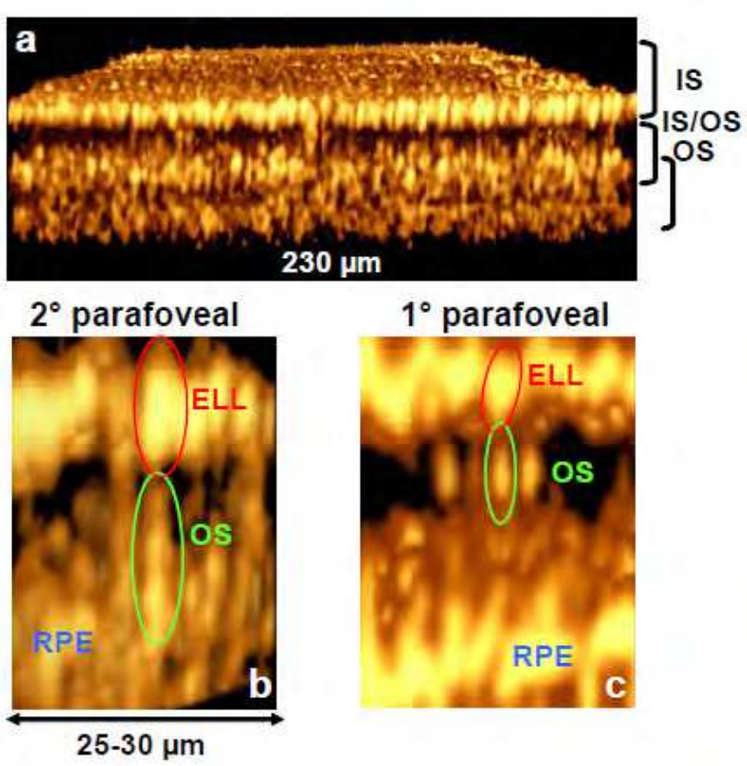

Fig. 15. In vivo cellular resolution retinal imaging at ~2.25 deg eccentricity: (a). Three dimensional morphology of photoreceptor ellipsoids, together with the outer segments is visualized. Two different volumes showing the detailed micro-structural architecture of single photoreceptors at two eccentricities: ~2.25 and ~1.12 deg (b, c).

employed two deformable mirror to enhance the correcting capability of aberration for AO-OCT system (RobertJ. Zawadzki, et al 2007). Barry Cense et al combined polarization-sensitive optical coherence tomography with adaptive optics to research birefringent of nerve fiber laye (Barry Cense, et al, 2009). The 3-D image of retinal photoreceptor has been achieved in vivo which is shown in Fig. 15 (Enrique J. Fernández, et al, 2008). In Fig. 15(a), the 3-D structure of the ellipsoids, together with the OS, was recognizable. This opens the door to study the possible connection between pathologies associated to the loss or alteration of photoreceptor elements, including the internal process of renewing photoactive discs. With development of AO-OCT technology, more and more retinal cells will be achieved 3-D imaging in vivo, and will provide a powerful imaging tool for establish the relationships between the disease with retinal image at 3-D cellular level.

6. Conclusion

This chapter provides a technical overview of the AO-OCT for ophthalmic imaging. The overview includes a detailed description of Zernike modes wave front aberration, Hartmann-Shack wave front sensor, the fundamental of adaptive optics technology, and the development process of AO-OCT technology. OCT provides the high axial resolution, and AO the complementary high transverse resolution. Combined AO with OCT, will achieve 3-D ultrahigh resolution, and it have realized 2-D and 3-D image of signal photoreceptor. The AO-OCT musters a potentially powerful imaging tool whose 3-D resolution and sensitivity in the eye can substantially surpass those of any current retinal imaging modality. However, most of the AO system is not only expensive but also larger diameter devices, resulting in AO-OCT system have a big size. Although the invention of MEMS deformable mirror reduces the size of AO-OCT system, its small stroke limits its ability of aberration correction. Therefore, in the future to invent a smaller aperture, larger stroke and cheaper wave front sensor is the critical issue.

7. Acknowledgment

This research was supported by the National Science Foundation of China (Grant No. 61108082), the Knowledge Innovation Program of the Chinese Academy of Sciences (Grant No.KGCX2-Y11-920)

8. References

A. Unterhuber, B. Povazˇ ay, B. Hermann, et al. (2003). Compact, low-cost Ti: Al2O3 laser for in vivo ultrahigh-resolution optical coherence tomography. *Optics Letters.,* Vol. 28, No.11, pp 905-907.

A.M. Rollins, M.D. Kulkarni, S. Yazdanfar, et al. (1998). In vivo video rate optical coherence tomography. *Optics Express.,* Vol. 3, No. 6, pp 219–229.

A.Roorda, F. Romero-Borja, W. Donnelly Iii, H. Queener, T. J. Hebert, and M. C. W. Campbell. (2002). Adaptive optics scanning laser ophthalmoscopy. *Opt. Express.,* Vol. 10, pp 405–412

Austin. Roorda & DavidR.Williams. (1999). The arrangement of the three cone classes in the living human eye. *NATURE.,* Vol. 397

B. Hermann, E. J. Fernández, A. Unterhuber, H. Sattmann, A. F. Fercher, W. Drexler, P. M. Prieto, and P. Artal. (2004). Adaptive optics ultrahigh resolution optical coherence tomography. *Opt. Lett.,* Vol. 29, pp 2142-2144

Barry Cense, Weihua Gao1, Jeffrey M. Brown, et al. (2009). Retinal imaging with polarization-sensitive optical coherence tomography and adaptive optics. *Opt. Express.,* Vol. 17, No. 24

Born. M and Wolf. E, (1980), Principles of Optics 7th edn , Publishing hourse of electronics industry, ISBN 7-121-01256-1, Beijin, China

Brett E. Bouma, Guillermo J. Tearney. (2002), Handbook of optical coherence tomography, Marcel Dekker, Inc. ISBN 0-8247-0558-0, Newyork, USA

D. Huang, E. A. Swanson, C. P. Lin, et al. (1991). Optical coherence tomography. *Science.,* Vol. 254, No. 5035, pp 1178-1181.

D. S. Adler, T.H. Ko, A.K. Konorev, et al. (2004). Broadband light source based on quantµm-well superlµminescent diodes for high-resolution optical coherence tomography. *Quantµm Electronics.,* Vol. 34, No. 10, pp 915-918.

D. T. Miller, D. R. Williams, G. M. Morris, and J. Liang. (1996). Images of cone photoreceptors in the living human eye. *Vision Res.,* Vol. 36, pp 1067–1079

D. T. Miller, J. Qu, R. S. Jonnal, and K. E. Thorn. (2003). Coherence Gating and Adaptive Optics in the Eye. *Proceedings of SPIE.,* Vol. 4956, pp 65-72

David Merino and Chris Dainty et al. (2006). Adaptive optics enhanced simultaneous en-face optical coherence tomography and scanning laser ophthalmoscopy. *Optics Express.,* Vol. 14, pp 3345-3353

E.J. Fernandez, B. Povazˇ ay, B. Hermann, et al. (2005). Three-dimensional adaptive optics ultrahigh-resolution optical coherence tomography using a liquid crystal spatial light modulator. *Vision Research.,* Vol. 45, No. 28, pp 3432-3444.

Enrique J. Fernández, Boris Hermann, Boris Považay, et al. (2008). Ultrahigh resolution optical coherence tomography and pancorrection for cellular imaging of the living hµman retina. *Opt. Express.,* Vol. 16, No. 15

Enrique J. Fernández, Boris Hermann, Boris Považay, et al. (2008). Ultrahigh resolution optical coherence tomography and pancorrection for cellular imaging of the living hµman retina, *Opt. Express.,* Vol. 16, No. 15

F. Lexer. (1999). Dynamic coherence focus OCT with depth-indenpent transversal resolution. *Journal of Modern Optics.,* Vol. 46, No. 3, pp 541-553.

Fried D L. (1977). Topical issue on adaptive optics. *Opt.Soc. Am.,*1977, Vol. 67, No. 3.

Guohua Shi, Yun Dai, Ling Wang, et al. (2008). Adaptive optics optical coherence tomography for retina imaging. *Chinese Optics Letters.,* Vol. 6, No. 6, pp 424-425

H.C. Howland. (1977). A subjective method for the measurement of monochromatic aberrations of the eye. *Journal of the Optical Society of America A.,* Vol. 67, No. 11, pp 1508–1518.

Heidi Hofer, Pablo Artal, Ben Singer, Juan Luis Aragón, and David R. Williams. (2001). Dynamics of the eye's wave aberration. *JOSA A.,* Vol. 18, No. 3, pp. 497-506

J. Liang, B. Grimm, S. Goelz, and J. F. Bille. (1994). Objective measurement of wave aberrations of the human eye with use of a Hartmann–Shack wave-front sensor. *J. Opt. Soc. Am. A.* Vol. 11, pp 1949–1957

J. Liang, D. R. Williams and D. T. Miller. (1997). Supernormal vision and high resolution retinal imaging through adaptive optics. *Journal of Optical Society of America A.,* Vol. 14, pp 2884-2892

J. Liang, D. R. Williams, and D. T. Miller. (1997). Supernormal vision and high-resolution retinal imaging through adaptive optics. *Opt. Soc. Am. A.,* Vol.14, pp 2884–2892

J.F. de Boer, B. Cense, B.H. Park, et al. (2003). Improved signal-to-noise ratio in spectral-domain compared with time-domain optical coherence tomography. *Optics Letters.,* Vol. 28, No. 21, pp 2067-2069

Junzhong Liang, Gerald Westheimer. (1993). Method for measuring visual resolution at the retinal level. *Opt. Soc. Am. A.,* Vol. 10, No. 8, pp 1691～1696

Ning Ling, Xuejun Rao, Zheping Yang, Cheng Wang. (2001). Wave front sensor for measurement of vivid hμman eye. *The 3rd International workshop on adaptive optics for industry and medicine.,* pp.85-90

R. C. Youngquist, S. Carr, and D. E. N. Davies. (1987). Optical coherence-domain reflectometry: a new optical evaluation technique. *Opt. Lett.* , Vol. 12, pp 158-160.

R. Leitgeb, C.K. Hitzenberger, A.F. Fercher. (2003). Performance of Fourier domain vs. time domain optical coherence tomography. *Optics Express.,* Vol. 11, No. 8, pp 889-894.

R. Zawadzki, S. Jones, S. Olivier, M. Zhao, B. Bower, J. Izatt, S. Choi, S. Laut, and J. Werner. (2005). Adaptive optics optical coherence tomography for high-resolution and high-speed 3-D retinal in vivo imaging. *Opt. Express.,* Vol. 13, pp 8532-8546

R.K.Tyson. (1991). Principles of adaptive optics. Academic PressInc, SanDiego,

Robert J. Zawadzki, Steven M. Jones, Scot S. Olivier, et al. (2005). Adaptive-optics optical coherence tomography for high-resolution and high-speed 3-D retinal in vivo imaging. *OPTICS EXPRESS.,* Vol. 13, No. 21

RobertJ. Zawadzki, StaceyS. Choi, Steven M. Jones, et al. (2007). Adaptive optics–optical coherence tomography: optimizing visualization of microscopic retinal structures in three dimensions. *J.Opt.Soc.Am.A.,* Vol. 24, No. 5

Shi Guohua, Ding Zhihua, Dai Yun, Rao Xunjun, Zhang Yudong. (2007). Adaptive optics optical coherence tomography. *Proceedings of SPIE.,* Vol. 6534, No. 1

Wenhan Jiang, Huagui Li. (1990). Hartmann-Shack wavefront sensing and wavefront control algorithm, *Proc.of SPIE.,* Vol. 1271, No. 82

Y. Zhang, J. Rha, R. S. Jonnal, and D. T. Miller. (2005). Adaptive optics spectral optical coherence tomography for imaging the living retina. *Opt. Express.,* Vol. 13, pp 4792-4811

Y. Zhang, S. Poonja, and A. Roorda. (2006). MEMS-based adaptive optics scanning laser ophthalmoscopy. *Opt. Lett,.* Vol. 31, pp 1268–1270

Yan Zhang, Barry Cense, Jungtae Rha, et al. (2006). High-speed volμmetric imaging of cone photoreceptors with adaptive optics spectral-domain optical coherence tomography. *Opt. Express.,* Vol. 14, No. 10, pp 4380-4394

Yimin Wang, Yonghua Zhao, Hongu Ren, et al. (2003). Ultrahigh resolution optical coherence tomography using continuμm generation from a photo crystal fiber. Coherence Domain Optical Methods and Optical Coherence Tomography in Biomedicine, *Proceedings of SPIE.,* Vol. 4956

Yudong Zhang, Ning Ling, Xuejun Rao, Xingyang Li, Cheng Wang, Xuean Ma, Wenhan Jiang. (2001). A small adaptive opticl system on table for hμman retinal imaging. *The 3rd International workshop on adaptive optics for industry and medicine.,* pp 97～104

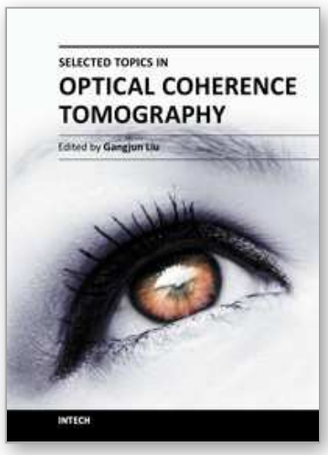

Selected Topics in Optical Coherence Tomography

Edited by Dr. Gangjun Liu

ISBN 978-953-51-0034-8
Hard cover, 280 pages
Publisher InTech
Published online 08, February, 2012
Published in print edition February, 2012

This book includes different exciting topics in the OCT fields, written by experts from all over the world. Technological developments, as well as clinical and industrial applications are covered. Some interesting topics like the ultrahigh resolution OCT, the functional extension of OCT and the full field OCT are reviewed, and the applications of OCT in ophthalmology, cardiology and dentistry are also addressed. I believe that a broad range of readers, such as students, researchers and physicians will benefit from this book.

INTECH
open science | open minds

InTech Europe
University Campus STeP Ri
Slavka Krautzeka 83/A
51000 Rijeka, Croatia
Phone: +385 (51) 770 447
Fax: +385 (51) 686 166
www.intechopen.com

InTech China
Unit 405, Office Block, Hotel Equatorial Shanghai
No.65, Yan An Road (West), Shanghai, 200040, China
中国上海市延安西路65号上海国际贵都大饭店办公楼405单元
Phone: +86-21-62489820
Fax: +86-21-62489821

IntechOpen